



High Temperature Oxidation of Hot-Dip Aluminized T92 Steels

Muhammad Ali Abro¹ · Junhee Hahn² · Dong Bok Lee³

Received: 31 August 2017 / Accepted: 5 November 2017 / Published online: 13 March 2018
© The Korean Institute of Metals and Materials 2018

Abstract

The T92 steel plate was hot-dip aluminized, and oxidized in order to characterize the high-temperature oxidation behavior of hot-dip aluminized T92 steel. The coating consisted of Al-rich topcoat with scattered Al_3Fe grains, Al_3Fe -rich upper alloy layer with scattered (Al, Al_5Fe_2 , AlFe)-grains, and Al_5Fe_2 -rich lower alloy layer with scattered (Al_5Fe_2 , AlFe)-grains. Oxidation at 800 °C for 20 h formed ($\alpha\text{-Al}_2\text{O}_3$ scale)/(AlFe layer)/(AlFe₃ layer)/($\alpha\text{-Fe(Al)}$ layer), while oxidation at 900 °C for 20 h formed ($\alpha\text{-Al}_2\text{O}_3$ scale plus some Fe_2O_3)/(AlFe layer)/(AlFe₃ layer)/($\alpha\text{-Fe(Al)}$ layer) from the surface. During oxidation, outward migration of all substrate elements, inward diffusion of oxygen, and back and forth diffusion of Al occurred according to concentration gradients. Also, diffusion transformed and broadened AlFe and AlFe₃ layers dissolved with some oxygen and substrate alloying elements. Hot-dip aluminizing improved the high-temperature oxidation resistance of T92 steel through preferential oxidation of Al at the surface.

Keywords T92 steel · Surface modification · Oxidation · Hot-dipping · Aluminizing

1 Introduction

ASTM grade T92 is a ferritic-martensitic steel (Fe–9%Cr–1.8%W–0.5%Mo) microalloyed with Mn, V, Si, Nb, carbon, and nitrogen. Alloying elements play important roles in improving corrosion resistance and mechanical properties such as creep strength, hardness, and toughness. By replacing Mo in T91 steel (Fe–9%Cr–1%Mo) with W to increase the creep strength, T92 steel was developed. It is widely used in power plants, petrochemical plants, oil or gas processing, and chemical industries due to its high creep strength with good resistance against corrosion and oxidation at elevated temperatures. However, its service life and operating temperature are still limited by oxidation and creep, although high Cr provides oxidation resistance by forming Cr_2O_3 scale [1, 2]. To achieve the maximum

operation efficiency, oxidation-resistant coatings are therefore needed. Aluminum is a suitable coating element because it can form protective $\alpha\text{-Al}_2\text{O}_3$ scale not only in air but also in (H_2O , SO_2 , H_2S)-containing aggressive corrosive environments due to high thermodynamic stability of Al_2O_3 [3, 4]. Aluminum can be coated by hot-dipping, pack cementation [5, 6], sputtering, slurry deposition [7], cladding, and metal spraying [8, 9]. In particular, hot-dip aluminizing is a simple and cost-effective diffusion coating technique that can be applied onto diverse shapes. Hot-dip aluminizing is carried out by dipping steel substrate into molten Al bath for a certain length of time. Inter-diffusion between the steel substrate and molten Al typically produces Al-rich topcoat, outer FeAl_3 layer, and inner Fe_2Al_5 layer [10–12]. Hot-dipping parameters such as bath composition, time, temperature, and substrate can affect the property of aluminized layer. Also, microstructure, phase constitution, thickness, and hardness of the aluminized layer can change during oxidation at high temperatures. Various scales could form on the aluminized layer depending on oxidation condition such as heating temperature, time, and gas composition. However, few studies have examined the high-temperature oxidation characteristics of hot-dip aluminized T92 steels. Previously, substrates employed for aluminizing have been mostly carbon steels [10, 13–17], low alloyed steels [6, 18], Fe–Si alloys [19], and Fe–Cr(–Mo) alloys [11, 12, 20–23].

✉ Dong Bok Lee
dlee@skku.ac.kr

¹ Department of Mechanical Engineering, MUET, SZAB Campus, Khairpur Mir's 66020, Pakistan

² Center for Energy Materials Metrology, Korea Research Institute of Standards and Science, Daejeon 34113, Republic of Korea

³ School of Advanced Materials Science and Engineering, Sungkyunkwan University, Suwon 16419, Republic of Korea

Until now, systematic studies about high-temperature oxidation behavior of aluminized T92 steels are lacking, although aluminized alloys are frequently exposed to oxidative environments at high temperatures. Hence, the objective of this study was to determine the hardness and changes in microstructures and compositions of hot-dipped aluminized T92 steel during oxidation in air.

2 Experimental Procedure

Commercially available T92 steel plates with nominal composition of Fe–9Cr–1.8W–0.5Mo–0.45Mn–0.2V–0.06Si–0.07C–0.06N–0.05Nb in wt% were cut to $10 \times 5 \times 5 \text{ mm}^3$ sized coupons, ground to 1000 grit SiC finish, immersed in 10 vol% HCl to remove surface oxides, subjected to liquid flux treatment with 20 vol% (KCl + AlF_3 in 4:1 weight ratio) solution in water, dried, and immersed at 800 °C for 5 min in a molten aluminum crucible on top of which a solid flux (KCl + NaCl + AlF_3 in 2:2:1 weight ratio) was spread to protect the molten bath from oxidation. The hot-dip aluminized samples were pulled out from the

bath, cooled to room temperature, and further cleaned using 5 vol% HNO_3 solution to remove any flux adhered on the surface. They were then oxidized isothermally at 800 and 900 °C for 20 h in atmospheric air, and inspected with an optical microscope (OM), a field-emission scanning electron microscope (SEM) equipped with an energy-dispersive spectroscopy (EDS), an electron probe micro-analyzer (EPMA), and a high-power X-ray diffractometer (XRD) at 40 kV and 150 mA with Cu- $\text{K}\alpha$ radiation. For microstructural observation, polished samples were examined with electron-back scattered diffraction (EBSD), or etched with Keller's reagent for aluminized coating and Vilella's reagent for T92 substrate. Microhardness was measured using Vickers microhardness tester at room temperature after applying load of 100 g for 5 s.

3 Results and Discussion

EPMA/EBSD/XRD results of hot-dip aluminized T92 steel are shown in Fig. 1. The cross-sectional BSE image of unetched sample (Fig. 1a) revealed that the coating consisted

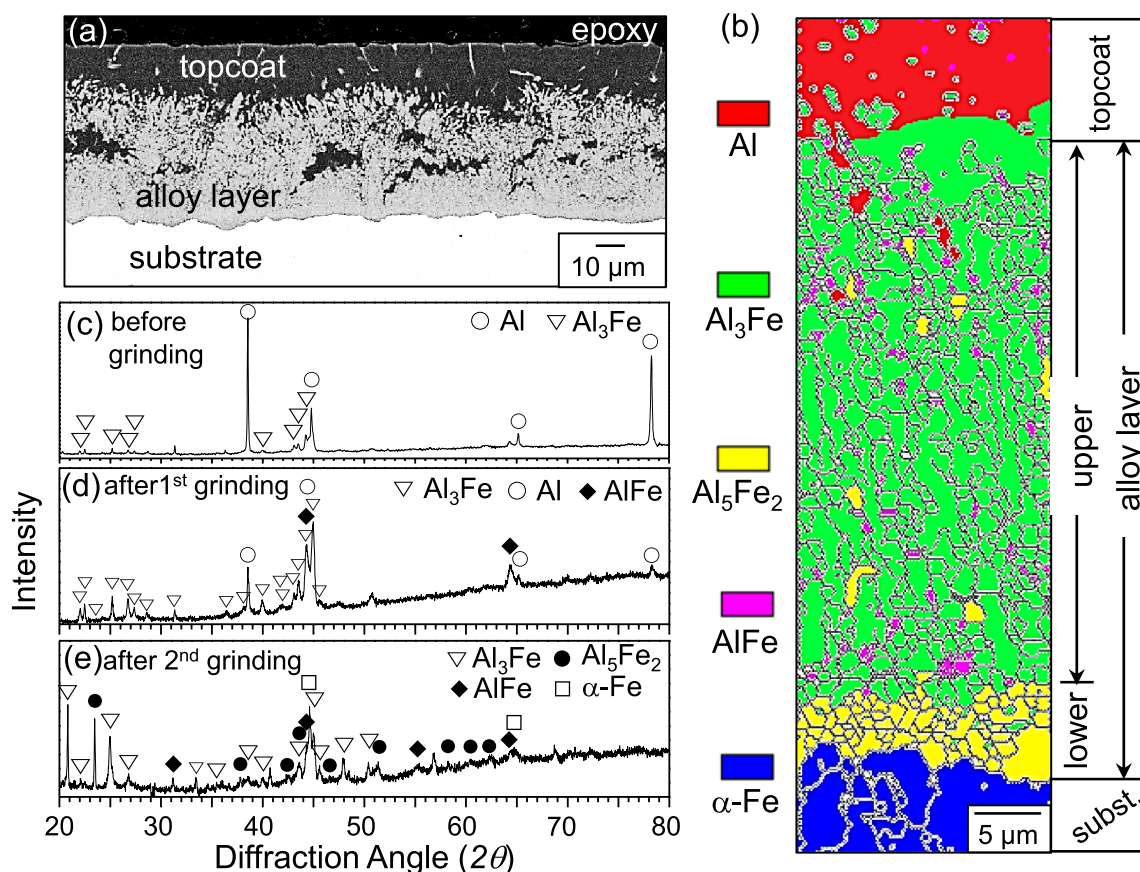


Fig. 1 Hot-dip aluminized T92 steel. **a** cross-sectional EPMA back-scattered electron (BSE) image (unetched), **b** EBSD phase/grain boundary distribution map, **c** XRD pattern before grinding, **d** XRD pattern after first grinding, **e** XRD pattern after second grinding

of ~ 15 μm -thick topcoat and ~ 45 μm -thick alloy layer. To identify coating phases, EBSD analysis (Fig. 1b) was performed. According to concentration gradient of Al and Fe arisen during hot dipping, the coating had the following characteristics. The Al-rich topcoat had a small amount of scattered Al_3Fe islands which precipitated out due to low solubility of Fe in Al. The alloy layer consisted of ~ 40 μm -thick Al_3Fe -rich upper layer and ~ 5 μm -thick Al_5Fe_2 -rich lower layer. A small amount of Al_5Fe_2 and AlFe islands scattered in the Al_3Fe -rich upper layer, wherein a small amount of Al islands additionally scattered. A small amount of Al_3Fe and AlFe islands scattered in the Al_5Fe_2 -rich lower layer. Grains in the Al_3Fe -rich upper layer tended to grow columnar along the counter-diffusion direction of Al and substrate elements, whilst those in the Al_5Fe_2 -rich lower layer were rather equiaxed (Fig. 1b). Such differences in grain morphology and thickness of each coating layer might be strongly associated with the non-stoichiometry and the amount of foreign substrate elements dissolved in Al–Fe phases, the inward diffusion rate of Al, and the outward diffusion rate of substrate elements. The phases constituting the hot-dipped coating are summarized in Table 1. The formation of (Al-rich topcoat)/(Al_3Fe layer)/(Al_5Fe_2 layer) from the surface has been similarly found in hot-dip aluminized carbon steels [14, 15, 17], high Si steel [19], 1.1Cr–0.25Mo steel [18], 5Cr–0.5Mo steel [20], 9Cr–1Mo steel [11], and 9.1Cr–1.4W steel [12]. Although the formation of (Al-rich topcoat)/(Al_3Fe layer only) was also reported in hot-dip aluminized Fe–12Cr [22], it is believed that Al_3Fe and Al_5Fe_2 are primary constituents in hot-dip aluminized steels due to their higher thermodynamic stability than Al_2Fe , FeAl, and AlFe₃ [16]. XRD results obtained before and after grinding off the sample surface on abrasive paper are shown in Fig. 1c–e. Strong Al peaks but weak Al_3Fe peaks were observed in Fig. 1c, suggesting that the topcoat consisted primarily of polycrystalline Al grains plus a small amount of Al_3Fe islands as reported previously [19]. Very strong Al_3Fe peaks, strong Al peaks, and moderate AlFe peaks were detected in Fig. 1d. In this result, Al came from the topcoat, while Al_3Fe and AlFe came from the upper alloy layer in which a small amount of AlFe islands were surrounded by numerous Al_3Fe grains. Very strong Al_3Fe peaks, strong (Al_5Fe_2 ,

$\alpha\text{-Fe}$)-peaks, moderate AlFe peaks were detected in Fig. 1e. In this result, $\alpha\text{-Fe}$ came from the substrate, Al_3Fe came mostly from the upper alloy layer, Al_5Fe_2 came mostly from the lower alloy layer, and AlFe came from the alloy layer. It has been reported that Al_8Cr_5 and AlCr_2 are also formed in hot-dip aluminized T91 steel in addition to Al_3Fe and Al_5Fe_2 [23]. However, such phases were not identified in this study.

The sample shown in Fig. 1 was analyzed further using EPMA/EDS. Results are shown in Fig. 2. In cross-sectional SE image of the unetched sample as shown in Fig. 2a, the Al-rich area was dark according to atomic contrast. The spot ① composition shown in Fig. 2b was 98.4Al–1.1Fe because a small amount of Al_3Fe scattered in the Al-rich topcoat (see Table 1). Hereafter, all compositions are expressed in atomic percentages (at.%). The spot ② composition was 76Al–23.2Fe–0.7Cr–0.1Mn because the Al_3Fe -rich upper alloy layer had a small amount of scattered Al, Al_5Fe_2 , and AlFe islands. The spot ③ composition was 71.5Al–25.7Fe–2.6Cr–0.1Mn–0.1W because the Al_5Fe_2 -rich lower alloy layer had a small amount of scattered Al_3Fe and AlFe islands. Alloying elements such as Cr, Mn, and W detected in spots ② and ③ were unrecognizable in Fig. 1c–e because they were dissolved in Al–Fe grains in the alloy layer (Fig. 1b). As moving deeper into the coating, substrate elements became richer, whereas Al became weaker according to concentration gradients (Fig. 2b). Overall distributions of Al and substrate elements are shown in Fig. 2c. In this result, Al_3Fe islands scattered in the Al-rich topcoat, and Cr and Mn dissolved in the Al–Fe alloy layer. However, W, Mo, Si, and V were hardly recognizable in the Al–Fe alloy layer due to their limited solubility or amount. The $\alpha\text{-Fe}$ substrate was virtually free from Al because the inwardly migrating Al was used up to form the coating. The dissolution of alloying elements in the Al_5Fe_2 -rich lower alloy layer smoothed the interface between the alloy layer and the substrate (Fig. 2a). When such dissolution occurred at a small extent as in the case of low-alloyed carbon steels, serrated tongue-like interface developed through fast diffusion of Al in orthorhombic Al_5Fe_2 with 30% vacancies along the c-axis, together with the formation of a relatively thick Al–Fe alloy layer [11, 13, 16]. Figure 2c indicates that alloying elements such as Cr and Mn partially occupied vacancies in Al_5Fe_2 to make the interface smooth, and reduced the thickening of the otherwise fast-growing Al_5Fe_2 alloy layer next to the substrate [24]. Depending on investigators, the Al_5Fe_2 -rich lower alloy layer has been found to be either thinner [20] or thicker [12, 14–16] than the Al_3Fe -rich upper alloy layer.

SEM/EDS/XRD/OM results of hot-dip aluminized T92 steel after oxidation at 800 °C for 20 h are shown in Fig. 3. Spots 1–3, 4, 5–8, 9–10, 11–13, and 14–15 denoted in Fig. 3a corresponded to the $\alpha\text{-Al}_2\text{O}_3$ scale, ($\alpha\text{-Al}_2\text{O}_3$, AlFe)-mixed layer, oxygen-affected AlFe layer, oxygen-affected AlFe₃ layer, Al-dissolved $\alpha\text{-Fe}$ layer (viz. $\alpha\text{-Fe(Al)}$), and

Table 1 Phases identified in the coating

after hot-dip aluminizing (Fig. 1)
topcoat; Al (major) + Al_3Fe islands (minor)
upper alloy layer; Al_3Fe (major) + Al, Al_5Fe_2 , AlFe islands (minor)
lower alloy layer; Al_5Fe_2 (major) + Al_3Fe , AlFe islands (minor)
after 800 °C/20 h oxidation (Fig. 3)
surface/coating/substrate; Al_2O_3 /AlFe/AlFe ₃ / $\alpha\text{-Fe(Al)}$ / $\alpha\text{-Fe}$
after 900 °C/20 h oxidation (Fig. 4)
surface/coating/substrate; (Al_2O_3 + Fe_2O_3)/AlFe/AlFe ₃ / $\alpha\text{-Fe(Al)}$ / $\alpha\text{-Fe}$

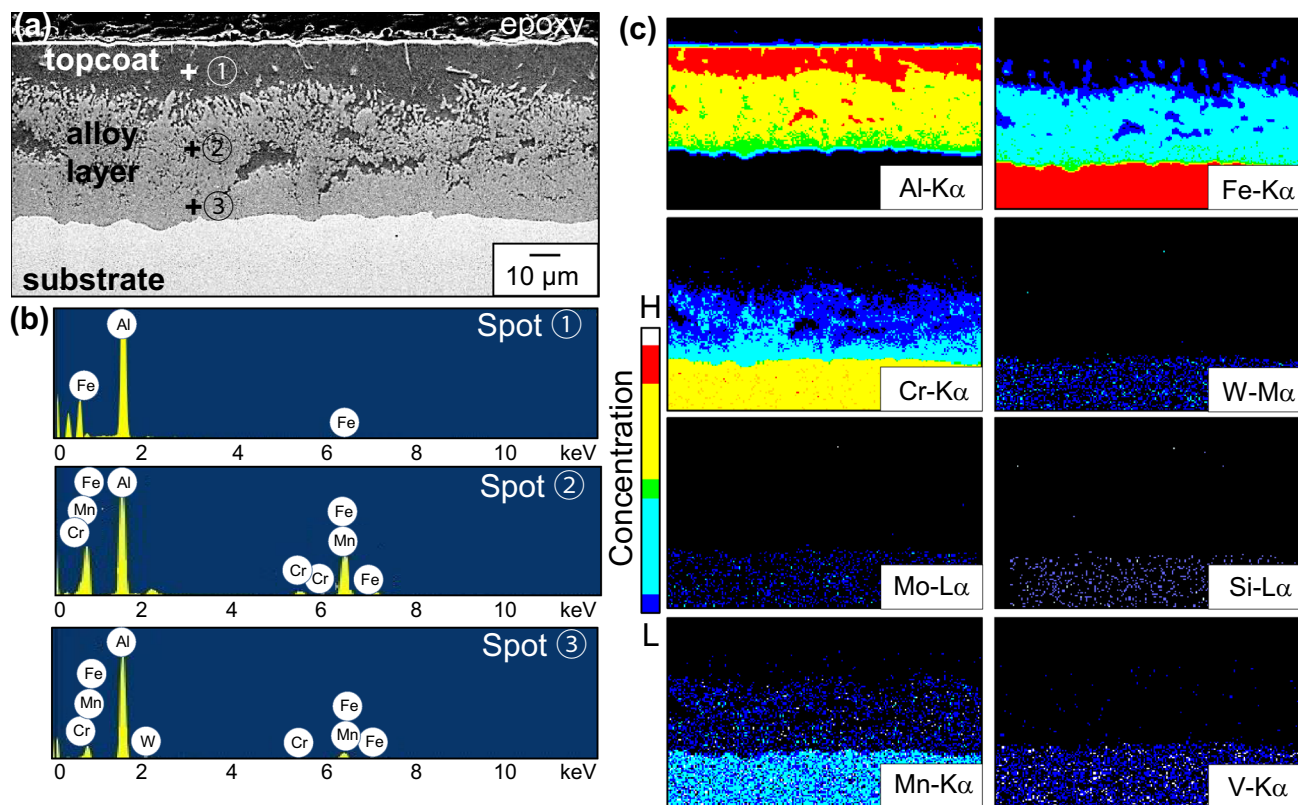


Fig. 2 Hot-dip aluminized T92 steel. **a** cross-sectional EPMA secondary electron (SE) image (unetched), **b** EDS spectra of ①, ②, and ③ marked in (a), and **c** EPMA maps of (a)

the original α -Fe substrate, respectively (Fig. 3b). Brittle Al_3Fe and Al_5Fe_2 identified in Fig. 1c–e were transformed to ductile AlFe and AlFe_3 through counter-diffusion of Al and Fe during heating. The α - Al_2O_3 surface scale and the underlying AlFe layer were detected in XRD patterns as shown in Fig. 3c, d. The average composition of spots 1–3 analyzed by FE-SEM/EDS was 58.5Al–39.2O–2.1Fe–0.2Cr (Fig. 3b). However, measured Al–O composition did not match with Al_2O_3 composition because spots 1–2 were at the edge of the scale. Nonetheless, the dissolution of foreign cations in α - Al_2O_3 and mismatch of thermal expansion coefficient of α - Al_2O_3 with the underlying AlFe layer made the scale somewhat thick and prone to spallation or breakage (Fig. 3a). The scale failure resulted in the detection of weak α - Al_2O_3 peaks but strong AlFe peaks (Fig. 3c). In Fig. 3b, spot 4 composition was 48.7Al–40Fe–8.1O–2.5Cr–0.4Mn–0.1W–0.1V–0.1Si due to the formation of (α - Al_2O_3 , AlFe)-mixed layer. The average composition of spots 5–8 was 44.9Al–44.6Fe–5.3O–4.4Cr–0.3Mn–0.2W–0.2V–0.1Si, indicating the dissolution of oxygen and substrate alloying elements in AlFe grains. The average composition of spots 9–10 was 25.1Al–62Fe–4O–7.8Cr–0.4Mn–0.5W–0.2V, suggesting the dissolution of oxygen and substrate alloying elements in AlFe_3 grains. The average composition of

spots 11–13 was 3.4Al–82.3Fe–3.3O–9.4Cr–0.6Mn–0.5W–0.2V–0.3Si, indicating the dissolution of oxygen and Al in α -Fe substrate to form the oxygen-affected α -Fe(Al) layer. Aluminum and oxygen were absent at spots 14–15 (i.e. the original α -Fe substrate), because they were used up at spots 1–13 (Fig. 3b). In Fig. 3e, some of the α - Al_2O_3 scale was detached off (*see* spot 1 in Fig. 3a). The adherent α - Al_2O_3 scale consisted of fine grains, reflecting its slow growth rate (Fig. 3e). Its position corresponded to spots 2–3 in Fig. 3a. The (α - Al_2O_3 , AlFe)-mixed thin layer denoted in Fig. 3e corresponded to spot 4 in Fig. 3a. Its grains were still fine because intermixed α - Al_2O_3 grains deterred the rapid growth of AlFe grains. The AlFe layer denoted in Fig. 3e corresponded to spots 5–8 in Fig. 3a. It consisted of columnar AlFe grains dissolved with oxygen and substrate alloying elements. The AlFe_3 layer denoted in Fig. 3e corresponded to spots 9–10 in Fig. 3a. It was hardly etched with Keller's and Vilella's reagent due to high Cr dissolved in AlFe_3 . The α -Fe(Al) layer and α -Fe substrate denoted in Fig. 3e corresponded to spots 11–13 and 14–15 in Fig. 3a, respectively. Their grain morphology was similar to each other (Fig. 3e). The coating initially consisted of ~ 15 μm -thick Al-rich topcoat and ~ 45 μm -thick alloy layer (Fig. 1). The Al-rich topcoat was partially oxidized to highly stable α - Al_2O_3

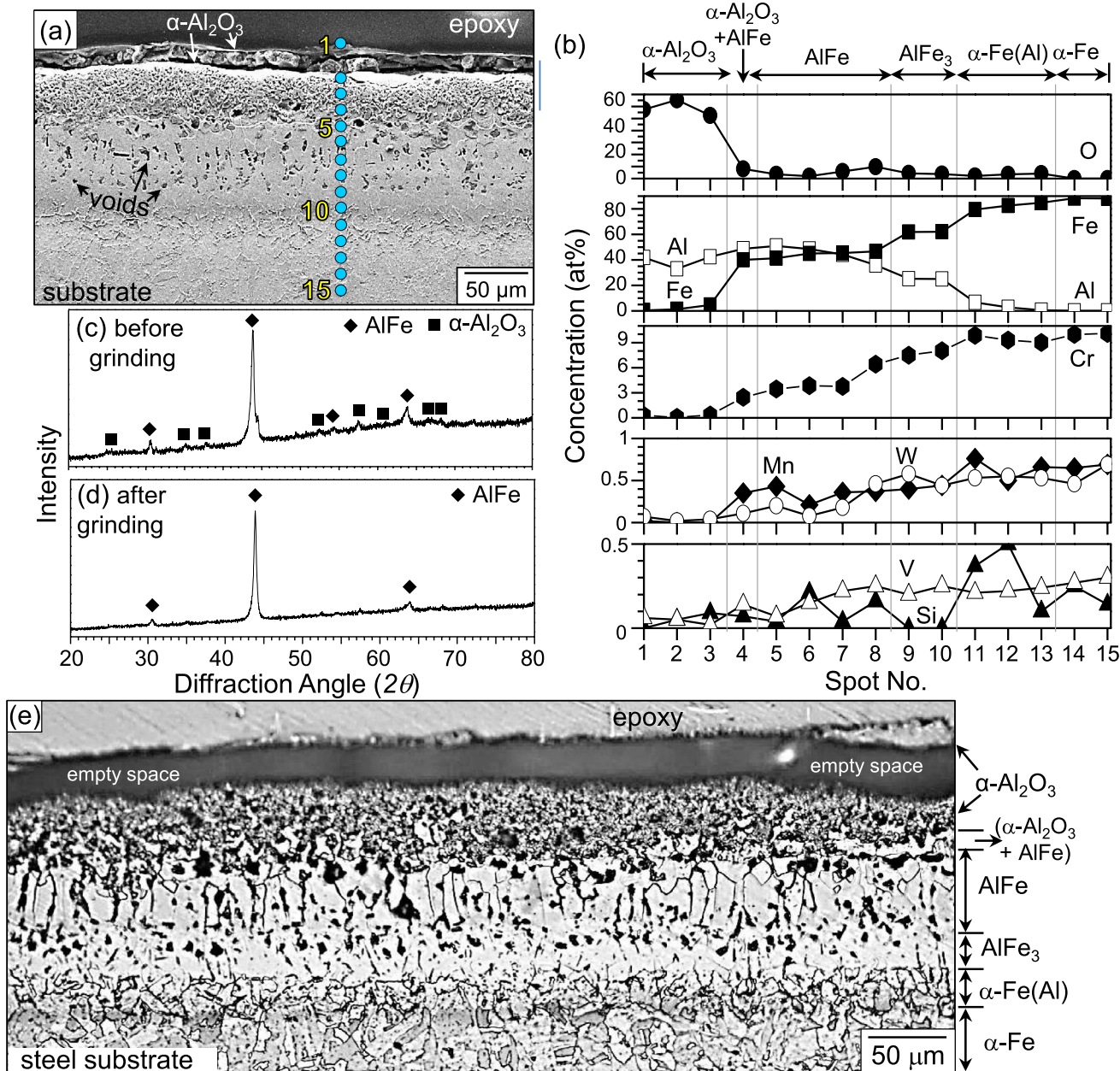


Fig. 3 Hot-dip aluminized T92 steel after oxidation at 800 °C for 20 h. **a** cross-sectional SEM SE image (etched), **b** EDS concentration profiles along spots 1–15 marked in (a), **c** XRD pattern before

grinding, **d** XRD pattern after grinding the coating surface, **e** cross-sectional OM image (etched)

scale (Fig. 3). The remaining Al-rich topcoat and the original Al–Fe alloy layer plus the adjacent substrate shown in Fig. 1a were transformed to ~14 μm-thick (α-Al₂O₃, AlFe)-mixed layer, ~54 μm-thick AlFe layer, ~20 μm-thick AlFe₃ layer, and ~23 μm-thick α-Fe(Al) layer as shown in Fig. 3e. Such substantial increase in coating thickness and transformation of Al–Fe phases resulted from the counter-diffusion of Al and substrate elements during heating in air.

When hot-dip aluminized T92 steel was oxidized further at 900 °C for 20 h, (α-Al₂O₃, Fe₂O₃)-mixed

oxide layer, AlFe layer, AlFe₃ layer, and α-Fe(Al) layer formed on the α-Fe substrate. This led to the detection of (α-Al₂O₃ + Fe₂O₃ + AlFe), AlFe₃, and (AlFe₃ + α-Fe) in Fig. 4a–c, respectively. In Fig. 4d, spots 1–2, 3–5, 5–9, 10, and 11 corresponded to the (α-Al₂O₃, Fe₂O₃)-mixed layer, AlFe layer, AlFe₃ layer, α-Fe(Al), and α-Fe layer, respectively. Such can be seen from the FE-SEM/EDS result shown in Fig. 4e, EPMA maps shown in Fig. 4f, and etched OM image shown in Fig. 4g. The average composition of spots 1–2 obtained from Fig. 4e was

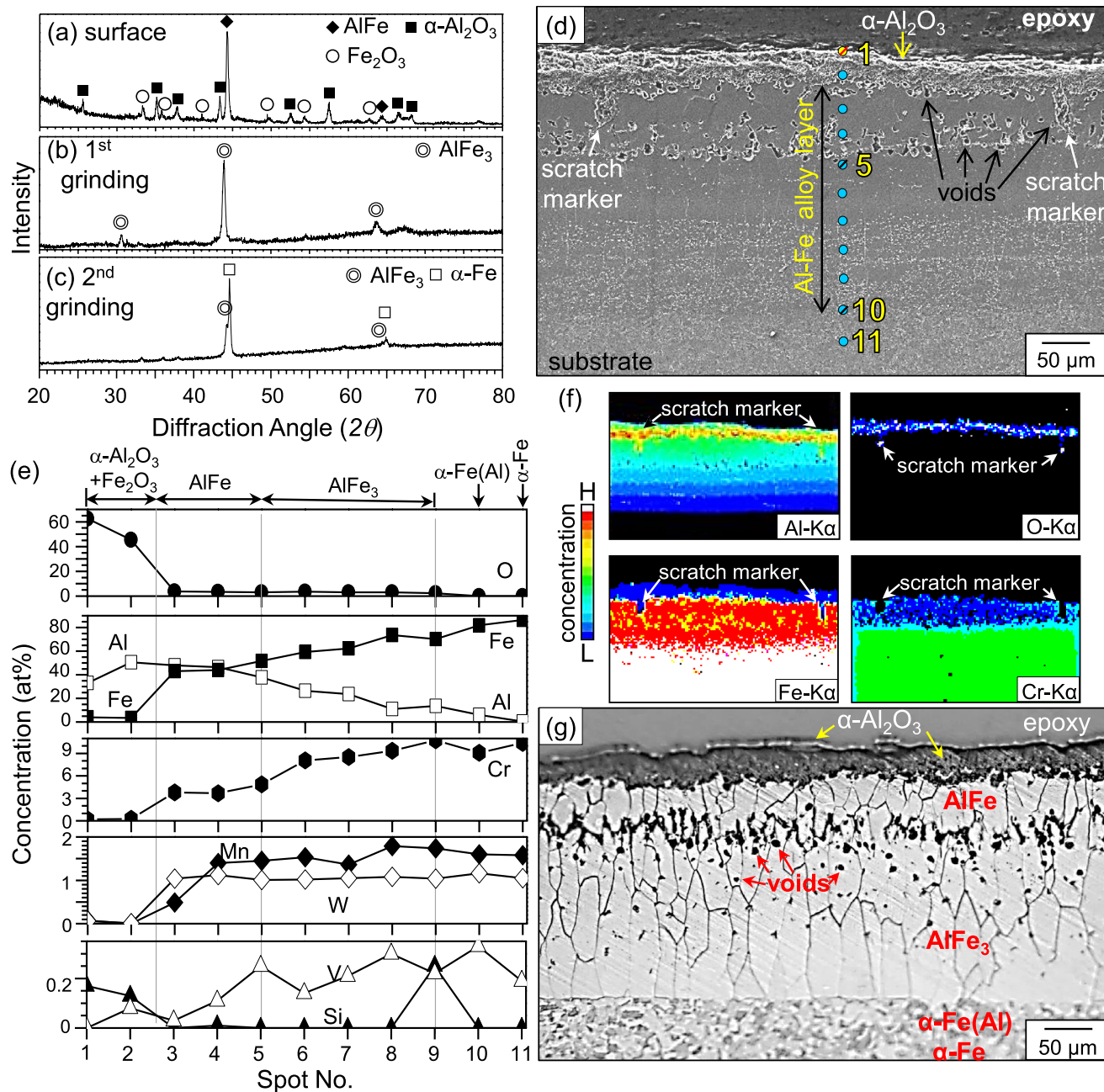


Fig. 4 Hot-dip aluminized T92 steel after oxidation at 900 °C for 20 h. **a** XRD pattern before grinding, **b** XRD pattern after first grinding, **c** XRD pattern after second grinding, **d** cross-sectional EPMA

SE image (etched), **e** EDS concentration profiles along spots 1–11 shown in **(d)**, **f** EPMA mappings of **(d)**, **g** cross-sectional OM image (etched)

39.2Al–56.8O–3.7Fe–0.2Cr–0.1Si, indicating that α -Al₂O₃ was the major phase while Fe₂O₃ was the minor one. This result might be due to the high diffusivity, strong oxygen affinity, and abundance of Al in the topcoat when compared to Fe that continuously diffused outwardly to the topcoat during heating. The average composition of spots 3–5 was 44Al–46.2Fe–3.4O–4.1Cr–1.1Mn–1.1W–0.1V, indicating that the AlFe layer was dissolved with some amounts of oxygen and substrate alloying elements such as Cr, Mn, W,

and V. That of spots 6–9 was 18.6Al–66.3Fe–3O–9.2Cr–1.6Mn–1.1W–0.2V, indicating that the AlFe₃ layer was dissolved with less oxygen but more substrate alloying elements than the overlying AlFe layer. The composition of spot 10 was 81.8Fe–6Al–9.1Cr–1.6Mn–1.2W–0.3V, indicating the dissolution of a large amount of Cr and Al in the oxygen-free α -Fe(AI) layer. Spot 11 composition was 86.4Fe–0.4Al–10.4Cr–1.6Mn–1W–0.2V, indicating that a small amount of Al diffused down to the oxygen-free α -Fe substrate. In

order to trace the original surface of the sample, the sample surface was scratched twice using a knife prior to oxidation (Fig. 4d). After oxidation, scratch markers were filled with $\alpha\text{-Al}_2\text{O}_3$ plus some Fe_2O_3 (Fig. 4f). Results indicated that, besides the inward transport of Al from coating, Al and some Fe diffused outwardly to be oxidized during oxidation, which left Kirkendall voids in the AlFe layer. The density decrement that occurred due to transformation of high-Fe phase to high-Al phase might have also assisted the formation of voids. The alloying element Cr with a high m.p. was not diffused into the scratch yet (Fig. 4f). During oxidation, Al in the coating diffused inwardly and outwardly [10], substrate elements diffused outwardly into the coating, and oxygen diffused inwardly according to concentration gradients. Grains in the coating were clearly revealed in Fig. 4g. In this result, the $\alpha\text{-Al}_2\text{O}_3$ layer with some Fe_2O_3 was $\sim 45\ \mu\text{m}$ -thick, consisting of fine oxide grains. The AlFe layer was $\sim 75\ \mu\text{m}$ -thick, consisting of short columnar grains. The AlFe_3 layer was $\sim 120\ \mu\text{m}$ -thick, consisting of coarse, more columnar grains. The $\alpha\text{-Fe}(\text{Al})$ layer had a thickness of $\sim 30\ \mu\text{m}$, and exhibited similar grain morphology with the $\alpha\text{-Fe}$ layer. In comparison with Fig. 3e, the incorporation of Fe_2O_3 grains in the $\alpha\text{-Al}_2\text{O}_3$ scale as well as the broadening of the AlFe_3 layer through enhanced counter-diffusion of Al and substrate elements due to increment of temperature was noticeable in Fig. 4g. Results obtained from Figs. 1, 2, 3, 4 are summarized in Table 1. In the case of hot-dip aluminized coating on 5Cr–0.5Mo steel, oxidation at $750\ ^\circ\text{C}$ for 10 h resulted in the formation of $\alpha\text{-Al}_2\text{O}_3/(\text{Al}_5\text{Fe}_2, \text{FeAl}_2)/\text{FeAl}$ layers on the substrate [20]. In the case of hot-dip aluminized coating on 1.1Cr–0.25Mo steel, oxidation at $850\ ^\circ\text{C}$ for 36 h resulted in the formation of $\alpha\text{-Al}_2\text{O}_3/\text{FeAl}_2/\text{FeAl}/\alpha\text{-Fe}(\text{Al})$ layers [18]. In the case of hot-dip aluminized coating on 9.1Cr–1.4W steel, oxidation at $960\ ^\circ\text{C}$ for 15 h resulted in the formation of $\alpha\text{-Al}_2\text{O}_3/\text{FeAl}_2/\text{FeAl}/\alpha\text{-Fe}(\text{Al})$ layers [12]. In the case of hot-dip aluminized coating on 0.24Mn steel, oxidation at $750\ ^\circ\text{C}$ for 24 h resulted in the formation of $\alpha\text{-Al}_2\text{O}_3/\text{Fe}_2\text{Al}_3/\text{FeAl}_2/\text{FeAl}$ layers [14, 15].

The beneficial effect of hot-dip aluminizing in improving the oxidation resistance of T92 steel was clearly seen from the comparison between Figs. 4 and 5. The oxidation condition was the same for both figures. Bare T92 steel was oxidized fast, forming $\sim 540\ \mu\text{m}$ -thick porous outer scale and $\sim 470\ \mu\text{m}$ -thick dense inner scale (Fig. 5a). The outer scale primarily consisted of Fe_2O_3 [25] (Fig. 5b). Alloying elements of T92 steel were mostly oxidized in the inner scale (Fig. 5c). Bright spots shown in Fig. 5a were Pd particles which were sprayed manually onto the sample surface prior to oxidation in order to determine the oxidation mechanism of bare T92 steel. The EPMA line profile of Pd is shown in Fig. 5c. This indicates that the outer oxide scale was formed primarily by outward diffusion of iron, which pushed Pd particles slightly upward through plastic flow. The ensuing

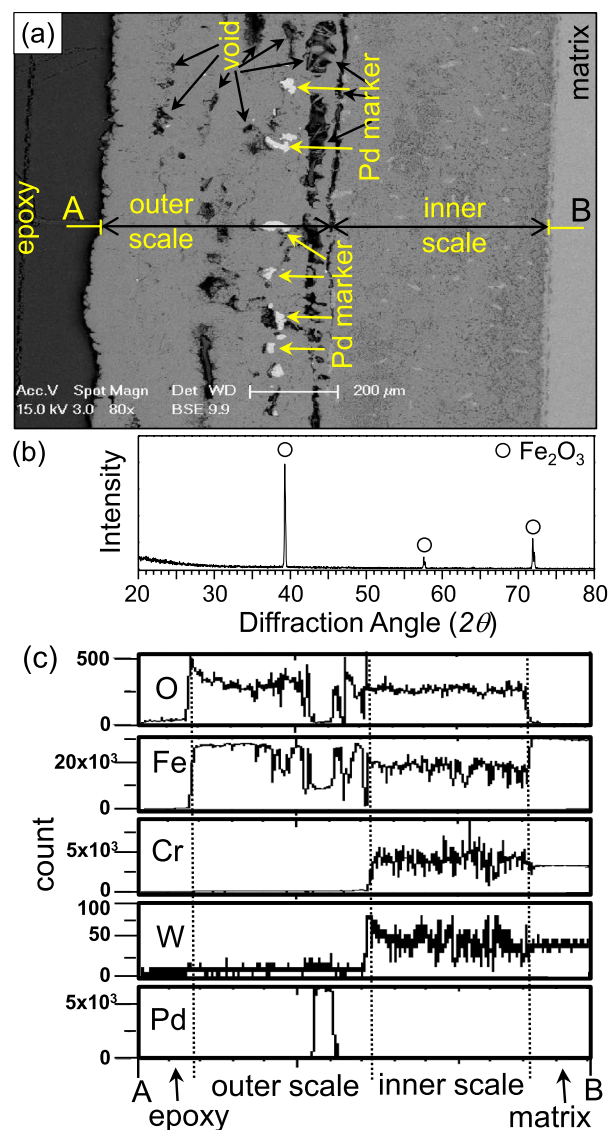


Fig. 5 T92 steel after oxidation at $900\ ^\circ\text{C}$ for 20 h. **a** EPMA cross-sectional BSE image, **b** XRD pattern, **c** EPMA line profile along A–B

outward diffusion of iron resulted in the formation of numerous Kirkendall voids in the outer scale (Fig. 5a). The inner oxide scale was formed by the inward migration of oxygen. Voids, including those interconnected at the interface of the outer and inner scale, and compositional difference between the outer and inner oxide scales caused the oxide scale with low plasticity to spall during cooling after oxidation.

Variation in Vickers hardness of hot-dip aluminized T92 steel along the depth is shown in Fig. 6. It was explained in Fig. 1 that the hot-dipped sample consisted of ($\sim 15\ \mu\text{m}$ -thick Al-rich topcoat), ($\sim 40\ \mu\text{m}$ -thick Al_3Fe -rich alloy layer), ($\sim 5\ \mu\text{m}$ -thick Al_5Fe_2 -rich alloy layer), and ($\alpha\text{-Fe}$ substrate). The average microhardness of (Al-rich topcoat), (Al_3Fe -rich alloy layer), (Al_5Fe_2 -rich alloy layer), and ($\alpha\text{-Fe}$ substrate) was 50, 686, 778, and 248 Hv, respectively (Fig. 6a). Since

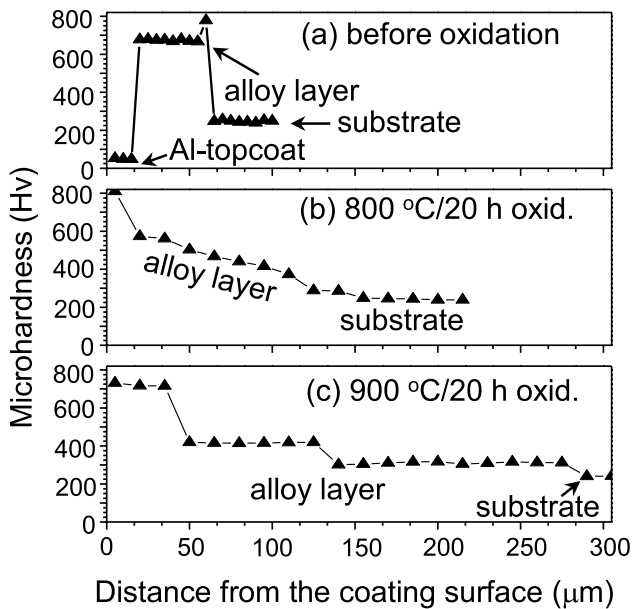


Fig. 6 Vickers microhardness along the depth of hot-dip aluminized T92 steel. **a** before oxidation, **b** after oxidation at 800 °C for 20 h, **c** after oxidation at 900 °C for 20 h

diffusion occurred nonuniformly even in one sample during hot-dipping and high-temperature oxidation, the thickness of each coating layer before and after oxidation varied at certain extent depending on the inspection area. It was explained in Fig. 3 that ~ 50 μm -thick $\alpha\text{-Al}_2\text{O}_3$ scale, ~ 54 μm -thick AlFe layer, ~ 20 μm -thick AlFe₃ layer, and ~ 23 μm -thick $\alpha\text{-Fe(Al)}$ layer formed on the $\alpha\text{-Fe}$ substrate.

Microhardness of AlFe and AlFe₃ has been reported to be 470 and 330 Hv, respectively [26]. The microhardness was found to decrease gradually (from 810 to 230 Hv) as moving deeper (Fig. 6b). It was explained in Fig. 4 that ~ 45 μm -thick $\alpha\text{-Al}_2\text{O}_3$ layer intermixed with some Fe₂O₃, ~ 75 μm -thick AlFe layer, ~ 120 μm -thick AlFe₃ layer, and ~ 30 μm -thick $\alpha\text{-Fe(Al)}$ layer formed on the $\alpha\text{-Fe}$ substrate. In Fig. 6c, the average microhardness (Hv) was approximately 721 for Al–Fe oxides, 417 for AlFe layer, 309 for AlFe₃ layer, 275 for $\alpha\text{-Fe(Al)}$ layer, and 240 for $\alpha\text{-Fe}$ substrate. Generally, heating softened the coating and the substrate. Factors that affected the hardness included the following: (1) Al–Fe alloy layers had dissolved oxygen and substrate alloying elements, which increased hardness through solid solution hardening, (2) heating at high temperatures decreased the hardness through grain growth and stress relieving, and (3) experimental error.

4 Summary

In order to elucidate the microstructural change of the aluminized T92 steel, Figs. 1a, 3e, and 4g are redisplayed at the same magnification in Fig. 7a–c, respectively. Our results showed that hot-dip aluminized coating consisted of topcoat, Al₃Fe-rich upper alloy layer, and lower Al₅Fe₂-rich alloy layer (Fig. 7a). In the alloy layer, a small amount of AlFe islands scattered. Grains of the Al₃Fe-rich layer were somewhat columnar while those of the Al₅Fe₂-rich layer were rather equiaxed (Fig. 7a). After oxidation at 800 °C for 20 h, $\alpha\text{-Al}_2\text{O}_3$ scale consisting of fine grains, AlFe layer consisting

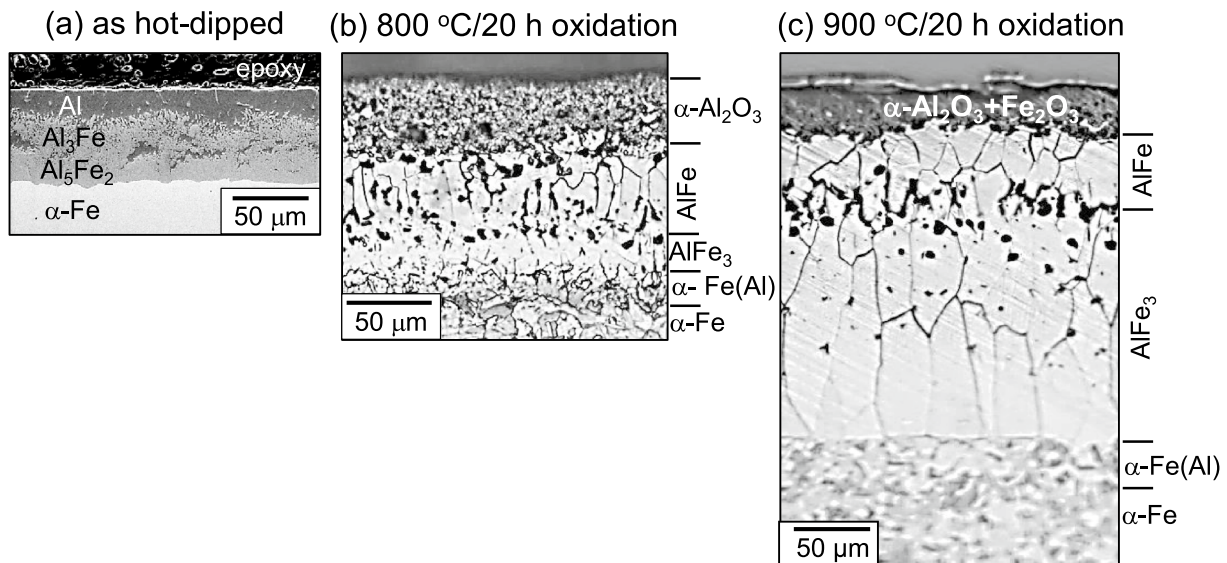


Fig. 7 Cross-sectional images of hot-dip aluminized T92 steel. **a** before oxidation, **b** after oxidation at 800 °C for 20 h, **c** after oxidation at 900 °C for 20 h

of columnar grains, AlFe₃ layer, and α-Fe(Al) layer formed on the α-Fe substrate (Fig. 7b). The α-Fe(Al) layer shared similar grain morphology with the α-Fe substrate. After oxidation at 900 °C for 20 h, α-Al₂O₃ scale with some Fe₂O₃, AlFe layer consisting of short columnar grains, AlFe₃ layer consisting of coarser, more columnar grains, and α-Fe(Al) layer formed on the α-Fe substrate (Fig. 7c). Preferential oxidation of Al-rich topcoat to α-Al₂O₃ scale effectively suppressed the oxidation. During oxidation, substrate elements diffused outwardly, Al migrated back and forth, and oxygen transported inwardly. In addition, voids formed in the alloy layer due to unequal mass flow and volume change caused by transformation of Al–Fe phases.

Acknowledgements This work was supported by the project “Development of the High-Efficiency Low-Emission Future Energy Production Technology (EO15580)” of National Research Council of Science and Technology (NST) grant by the Korea government (MSIP) (No. CRC-15-07-KIER).

References

1. M. Schütze, M. Schorr, D.P. Renusch, A. Donchev, J.P.T. Vossen, *Mater. Res.* **7**, 111 (2004)
2. K. Chandra, A. Kranzmann, R.S. Neumann, F. Rizzo, *Oxid. Met.* **84**, 463 (2015)
3. M.A. Abro, D.B. Lee, *Met. Mater. Int.* **23**, 92 (2017)
4. M.J. Kim, D.B. Lee, *Korean J. Met. Mater.* **53**, 406 (2015)
5. A.R. Rastkar, N. Rezvani, *Met. Mater. Trans.* **46A**, 4132 (2015)
6. Y.I. Son, C.H. Chung, R.R. Gowkanapalli, C.H. Moon, J.S. Park, *Met. Mater. Int.* **21**, 1 (2015)
7. A. Agüero, M. Gutiérrez, V. González, *Mater. High Temp.* **25**, 257 (2008)
8. M. Schütze, M. Malessa, V. Rohr, T. Weber, *Surf. Coat. Technol.* **201**, 3872 (2006)
9. R. Drewett, *Corros. Sci.* **9**, 823 (1969)
10. C.J. Wang, S.M. Chen, *Surf. Coat. Technol.* **200**, 6601 (2006)
11. W.J. Cheng, C.J. Wang, *Appl. Surf. Sci.* **277**, 139 (2013)
12. X. Chen, Q. Huang, Z. Yan, Y. Song, S. Liu, Z. Jiang, *J. Nucl. Mater.* **442**, S597 (2013)
13. C.J. Wang, M. Badaruddin, *Surf. Coat. Technol.* **205**, 1200 (2010)
14. W.J. Cheng, C.J. Wang, *Appl. Surf. Sci.* **257**, 4663 (2011)
15. W.J. Cheng, C.J. Wang, *Appl. Surf. Sci.* **277**, 258 (2013)
16. H.R. Shahverdi, M.R. Ghomashchi, S. Shabestari, J. Hejazi, *J. Mater. Process. Technol.* **124**, 345 (2002)
17. B. Lemmens, H. Springer, I.D. Graeve, J.D. Strycker, D. Raabe, K. Verbeken, *Surf. Coat. Technol.* **319**, 104 (2017)
18. M. Badaruddin, C.J. Wang, H. Wardono, Tarkono, D. Asmi, *AIP Conf. Proc.* **1711**, 0400021 (2016)
19. M.B. Lin, C.J. Wang, *Surf. Coat. Technol.* **205**, 1220 (2010)
20. W.J. Cheng, Y.Y. Chang, C.J. Wang, *Surf. Coat. Technol.* **203**, 401 (2008)
21. Y.Y. Chang, C.C. Tsaur, J.C. Rock, *Surf. Coat. Technol.* **200**, 6588 (2006)
22. J.H. Kim, J.P. Wang, C.Y. Kang, *Met. Mater. Int.* **17**, 931 (2011)
23. M. Emami, H.R. Shahverdi, S. Hayashi, M.J. Torkamany, *Metall. Mater. Trans. A* **44**, 3176 (2013)
24. G.H. Awan, F.U. Hasan, *Mater. Sci. Eng. A* **472**, 157 (2008)
25. P. Mathiazhagan, A.S. Khanna, *High Temp. Mater. Proc.* **30**, 43 (2011)
26. M.J. Rathod, M. Kutsuna, *Weld. J.* **83**, 16S (2004)